Spectral Impulse Noise Model for Spectral Image Processing

Hilda Deborah[1,2(✉)], Noël Richard[1], and Jon Yngve Hardeberg[2]

[1] Laboratory XLIM-SIC UMR CNRS 7252, University of Poitiers, Poitiers, France
hildad@hig.no
[2] The Norwegian Colour & Visual Computing Laboratory,
Gjøvik University College, Gjøvik, Norway

Abstract. The performance of an image processing algorithm can be assessed through its resulting images. However, in order to do so, both ground truth image and noisy target image with known properties are typically required. In the context of hyperspectral image processing, another constraint is introduced, i.e. apart from its mathematical properties, an artificial signal, noise, or variations should be physically correct. Deciding to work in an intermediate level, between real spectral images and mathematical model of noise, we develop an approach for obtaining suitable spectral impulse signals. The model is followed by construction of target images corrupted by impulse signals and these images will later on be used to evaluate the performance of a filtering algorithm.

Keywords: Hyperspectral image · Image processing · Impulse noise

1 Introduction

One way to evaluate the performance of an image processing algorithm is through its resulting images, and thus to employ full-reference image quality assessment (IQA). In order to conduct full-reference IQA, both reference and target images are required. Reference image will be image of an ideal case that is to be achieved by the algorithm. Target image is usually the modification of the reference image by certain criteria that is defined according to its application, e.g. filtering, segmentation, classification, etc. It is therefore by having the target image with known properties that we are able to measure the performance of image processing algorithms, e.g. stability, robustness, etc.

The performance of filtering algorithms are evaluated by means of signal/image denoising or frequency-band decomposition. However, for nonlinear filters, the relationship between spatial frequency and the parameters of the filters are not straightforward. Therefore, filtering performance is assessed through its performance in denoising task, given a certain noise model. Among the existing noise models, nonlinear impulse noise is most often used [2,5,8] as it models or approximates the malfunctioning pixels in camera sensor, transmission problems over a noisy channel, or faulty memory locations in data storage [6]. Interestingly,

A. Trémeau et al. (Eds.): CCIW 2015, LNCS 9016, pp. 171–180, 2015.
DOI: 10.1007/978-3-319-15979-9_17

Table 1. Notation

$I(x) = S$	Image function at location x, $I(x) \subset \mathbb{R}^n$
$\tilde{I}(x)$	An image disturbed by noise or unwanted variations
S	A spectrum describing image value at $I(x)$, $S = \{s_i,\ i \subset [1, n_c]\}$
n_c	Number of channels
$\overline{S}$	Average spectrum
$\mathfrak{S}$	A set of spectra, $\mathfrak{S} = \{S_i, i \subset [1, n_S]\}$
$\mathfrak{S}_n$	A set of candidate impulse signals
R	Random variable
r	Probability value of a pixel to be corrupted by impulse
T	Probability threshold
$\mathcal{N}$	Impulse signal
$\mathcal{H}(y)$	Heavyside function, $\mathcal{H}(y) = 1,\ \forall y > 0$
$d(S_1, S_2)$	Distance between 2 spectra S_1 and S_2
$\mu_d,\ \sigma_d$	Mean and standard deviation of distance
c	A constant number

even assuming a calibrated imaging system, in spectral image domain impulse noise is said to be ubiquitous [10]. It is therefore necessary to extend the model of impulse noise in the context of spectral image processing, and to do it correctly by taking a careful consideration of the nature of spectral data.

This article is organized as follows. Section 2 describes the existing impulse noise model that is widely used for grayscale and color images extended to spectral images. Furthermore, an extension to spectral images at an intermediate level which embeds mathematical model and real physical properties of noise is proposed. In Section 3 we study the characteristics of several pigment patches that were acquired by a hyperspectral scanner. The patches will then be used construct ground truth and noisy target images that will be used to assess the performance of a filtering algorithm in Section 4. The conclusion of this study is finally drawn in Section 5.

2 Impulse Noise Models

Impulse noise model was initially defined for grayscale image and is characterized by very large positive and negative values corrupting an image value for a short duration; these short-lived noise introduces speckles to an image. Impulse noise will then result in black and white spots in an image, hence the name *salt-and-pepper* noise. This noise model has uniform probability density function, i.e. a random variable R is independent and identically distributed over the image.

2.1 Salt-and-Pepper Noise

By definition there are two different models of salt-and-pepper noise, i.e. fixed and randomized noise signals [7]. In the case of grayscale image, fixed noise signals means that noise signals will be of value 0 or 1, while randomized signals

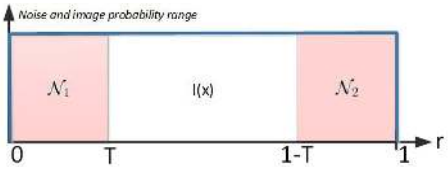

Fig. 1. The probability range of an image value being disturbed by an impulse

means that its value will lie between [0, 1]. The randomized approach has been used to extend this noise model to color image domain. In color image, impulse noise is modeled by randomly and independently generating the impulse in each color channel [4,9], causing the occurrences of false colored pixels. In other words, the extension of impulse noise to color image takes a marginal approach. To extend this model to spectral images, we choose to use a fixed signals approach rather than the randomized one. Two spectra $\mathcal{N}_1$ and $\mathcal{N}_2$ that are randomly generated will be used as noise signals corrupting an image value.

$$\mathcal{N}_k = \{s_i = y, i \subset [1, n_c], y \subset [0, 1]\} \tag{1}$$

As mentioned previously, this noise model has a uniform probability density function, see Fig. 1. The probability of having either $\mathcal{N}_1$ or $\mathcal{N}_2$ disturbing an image value is identical, i.e. $T_1 = 1 - T_2 = T$. Consequently, the probability of having an image value corrupted by impulse signals is $2T$. Finally, an image in the presence of impulse noise is classically described as follows:

$$\tilde{I}(x) = I(x) + \mathcal{H}\Big(T - r\Big)\Big(\mathcal{N}_1 - I(x)\Big) + \mathcal{H}\Big(r - 1 + T\Big)\Big(\mathcal{N}_2 - I(x)\Big) \tag{2}$$

2.2 Spectral Impulse Noise

Extending the construction of impulse noise to spectral images, especially hyperspectral image, induces a question whether the model is suitable for these images. Hyperspectral acquisition captures the physical composition of scenes or objects. The imaging system is calibrated and the acquired image is given after several corrections, e.g. radiometric, geometric, etc. Nevertheless, impulse noise is ubiquitous [10]. The origin of impulse signals in hyperspectral images might then be due to physical variations of the object itself or factors that affect photons arriving on the sensor.

Knowing that the impulse signals mostly originate from factors that happen before the sensor, it should rather be considered as spectral variations as opposed to spectral noise. Image examples in Fig. 2 show that variations that appear in uniform regions vary from the initial color by certain hues and magnitudes. With this consideration, we define a spectral impulse noise model that is not only a mathematical model but is also integrating the physical aspects of data by using a dataset of real impulse signals, where the noise signals $\mathcal{N}_1$ and $\mathcal{N}_2$ can be obtained by defining local constraints on the uniform regions.

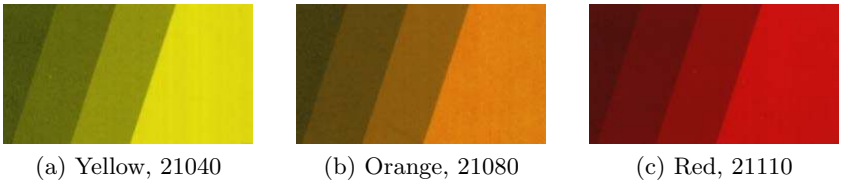

(a) Yellow, 21040 (b) Orange, 21080 (c) Red, 21110

(d) Blue, 44450 (e) Green, 44500 (f) Purple, 45120

Fig. 2. Pigment patches of several different color hues. In addition to having several hues, each of the hues are given in four different saturations.

The construction of dataset of real impulse signals is as follows. Given a uniform region of N_P pixels, in which the uniformity is defined as satisfying certain external criteria, we extract all the spectra within this uniform region forming a set of spectra $\mathfrak{S}$. For a specific uniform region, a subset of furthest spectra from the average spectrum is extracted, see Eq. 5 where c allows to reduce the subset size. Then, the candidate impulse signals are the two furthest signals obtained from within the subset, see Eq. 6.

$$\overline{S} = \frac{1}{N_P} \sum_{i=1}^{N_P} S_i \tag{3}$$

$$\mu_d = \frac{1}{N_P} \sum_{i=1}^{N_P} d(S_i, \overline{S}),\ \sigma_d = \sqrt{\frac{1}{N_P} \sum_{i=1}^{N_P} \big(d(S_i, \overline{S}) - \mu_d\big)^2} \tag{4}$$

$$\mathfrak{S}_n = \{S_i : d(S_i, \overline{S}) \geq (\mu_d + c \cdot \sigma_d), S_i \in \mathfrak{S}\} \tag{5}$$

$$(\mathcal{N}_1, \mathcal{N}_2) = \{ \underset{\forall (S_i, S_j) \in \mathfrak{S}_n^2}{\operatorname{argmax}} d(S_i, S_j)\} \tag{6}$$

3 Experimental Study and Discussion

More than 50 pigment patches of different hues were acquired using a pushbroom hyperspectral scanner HySpex [1]. This hyperspectral scanner provides data with 160 spectral bands in the range of 414.2 to 993.7 nm, in 3.6 nm interval. Some of the acquired images are shown in Fig. 2. In addition to hue variations, each patch comes with four different saturation levels. Spatial regions or pixels having the same hue and saturation level are defined as uniform region; further on, this

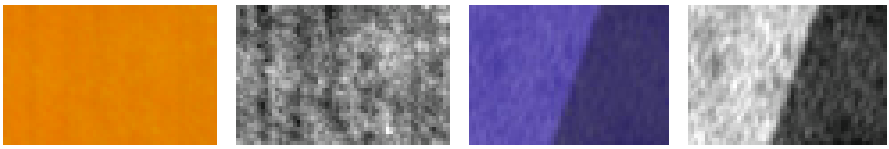

(a) 21080: Patch (b) 21080: Var. (c) 45120: Patch (d) 45120: Var.

Fig. 3. Cutouts of two pigment patches, showing variations in regions that are nevertheless defined as uniform regions

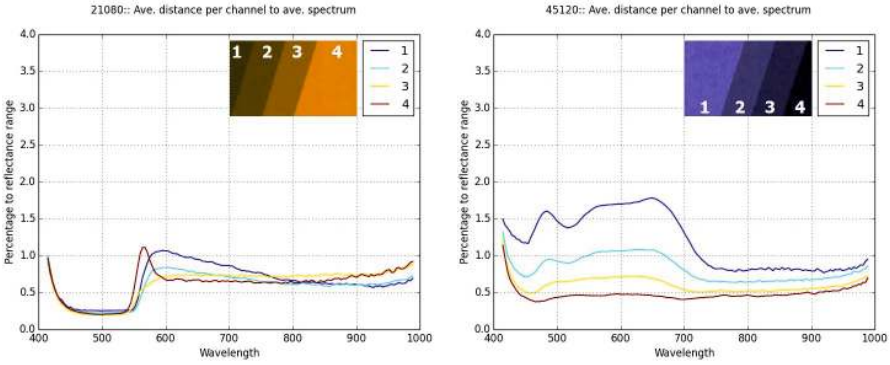

(a) Orange, 21080 (b) Purple, 45120

Fig. 4. Average spectral variations in original image computed channel-by-channel to the average spectrum for each pigment shade

uniform region will be referred to as *pigment shade*. Using the pigment patches we are able to obtain the dataset of impulse signals using the model explained in Section 2.2, as the patches provide us with uniform regions. Two impulse noise spectra $\mathcal{N}_1^k$ and $\mathcal{N}_2^k$ are therefore defined for each uniform region $\mathcal{R}^k$. With this noise generation, we are able to construct both ground truth and noisy target images required by full-reference image quality assessment in order to estimate the performance of spectral image processing algorithms.

3.1 Spectral Variations in Uniform Regions

By saying that each of the pigment shades is a uniform region, we are making a hypothesis that these regions are not textured. And consequently, spectral variations originating from physical composition of the materials, e.g. surface thickness and pigment density variations, are unwanted. The aforementioned variations can be observed in more details for several pigment patches in Fig. 3.

To investigate the distribution of spectral variations that exist in all pigment patches, we compute an average spectrum for each pigment shade giving four

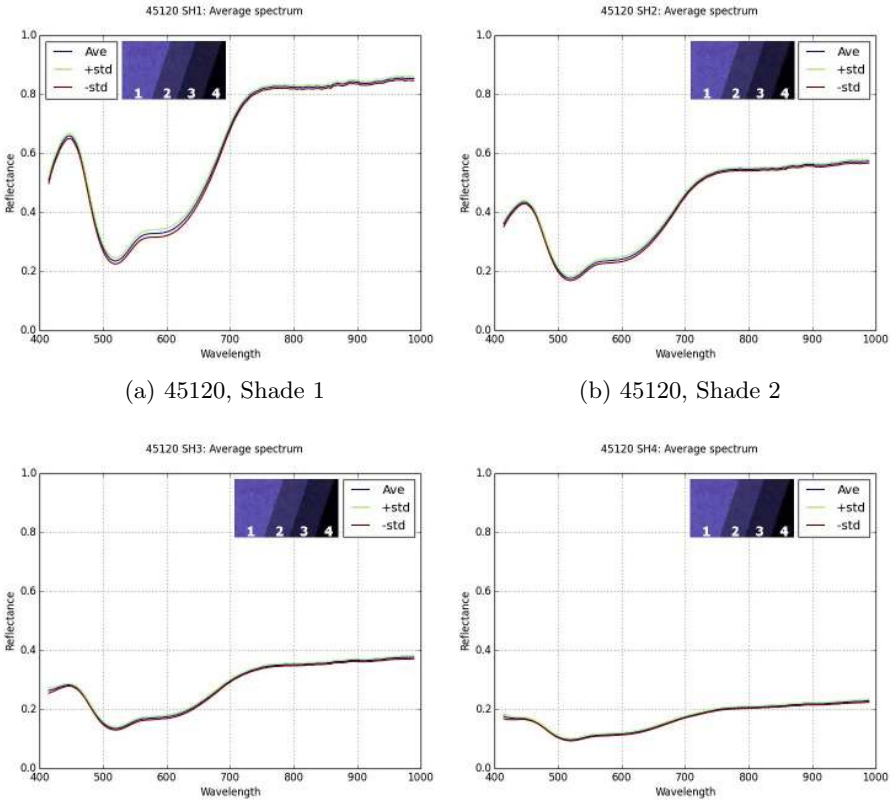

(a) 45120, Shade 1

(b) 45120, Shade 2

(c) 45120, Shade 3

(d) 45120, Shade 4

Fig. 5. Average spectrum for each shade in pigment patches 45120, and how spectra within these shades vary around the average spectrum

average spectra for each pigment patch; pixels located around edges are not taken into account. Spectral variations for all pixels in the image are then computed relative to its corresponding average spectrum, in terms of average and standard deviation of channel-by-channel difference. The average difference of several pigment patches to its respective average spectrum is provided in Fig. 4. By the two examples, we can observe that there is a lack of correlation between the magnitude of spectral variations and the spectral structures which correspond to hue and saturation differences. In Fig. 5 we can observe the magnitude of unwanted spectral variations to average spectrum of pigment 45120.

From this observation it can be seen that the magnitude of spectral variations cannot be predicted easily. It is certainly not independent from the choice of color or pigment and does not correlate to saturation; not to mention many other factors that have not been taken into account. Finally this observation lead us to take another hypothesis, i.e. each pigment spectrum has its particular unwanted

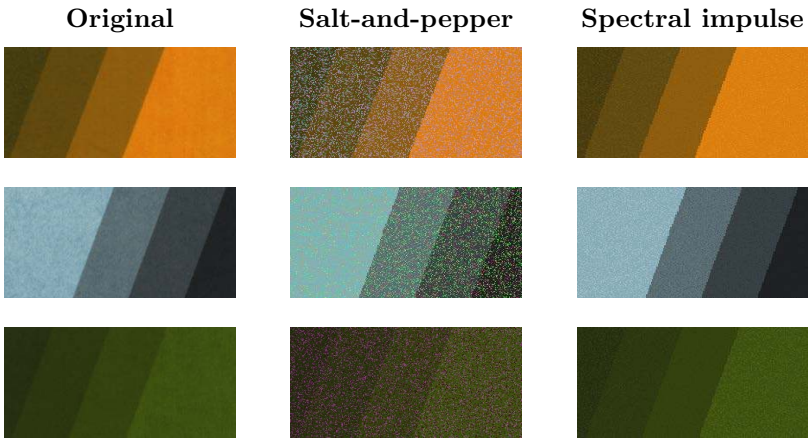

Fig. 6. Color images of several pigment patches acquired using a hyperspectral scanner and its corresponding artificial noisy images that are constructed using two impulse noise models with $T = 0.15$, i.e. salt-and-pepper and spectral impulse noise model.

spectral variations that are different from other spectra. Nevertheless, we can consider that between two spectra, the spectral variations can be interpolated knowing the nature of continuous world.

3.2 Artificially Noisy Pigment Patches

To obtain noisy spectral images required to evaluate the performance of spectral image processing algorithms, those that are with known properties and similar to real spectral images, the dataset of spectral impulse noise is used. We consider the proposed model described in Subsection 2.2 to be generic, although to this point it has only been investigated for water-based pigment that are applied to its substrate by screen-printing.

In Fig. 6 we can see the acquired images of several pigment patches and also its corresponding artificial target images. The target images were constructed using two models, i.e. salt-and-pepper and the proposed spectral impulse noise model, with probability threshold $T = 0.15$. Distortion measures relative to ground truth images are given for each pigment patch in Table 2. This table allows us to compare the distortion level of artificial target images constructed using the two different models. Salt-and-pepper model needs probability threshold $T < 0.05$ to have a similar distortion level to that of the acquired images. However, with such low amount of variations in a target image we will be unable to evaluate filtering performance, as the algorithm will perform the task perfectly. On the other hand with spectral impulse noise model, we can achieve a similar distortion level to that of the original image, i.e. with $T = [0.15, 0.2]$. Eventually by comparing the artificial target to acquired images, we can say that spectral impulse noise model is more realistic than salt-and-pepper.

Table 2. Distortion measures relative to ground truth images. The measures are given for originally acquired images and artificial target images constructed using salt-and-pepper and spectral impulse noise model. Values are given in unit of 10^{-3}.

Pigment patch	Original	Salt & pepper	Spectral impulse				
		$T = 0.05$	$T = 0.05$	0.1	0.15	0.2	0.25
Yellow, 21040	7.884	25.814	3.279	6.212	8.885	11.349	13.441
Orange, 21080	7.776	27.076	2.356	4.405	6.338	8.046	9.627
Red, 21110	7.875	24.936	2.514	4.799	6.877	8.759	10.398
Blue, 44450	10.868	21.383	3.983	7.553	10.871	13.766	16.538
Green, 44500	7.565	23.917	2.333	4.467	6.418	8.144	9.745
Purple, 45120	8.789	21.615	2.810	5.348	7.645	9.701	11.667

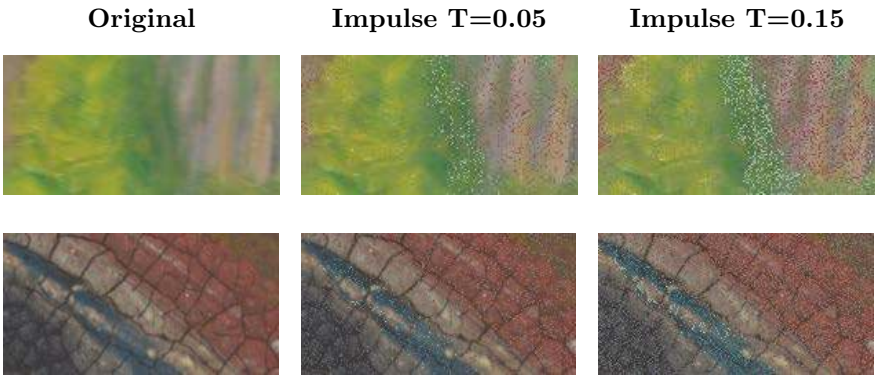

Fig. 7. Two cutouts taken from hyperspectral images of two different paintings. Original images are provided in the leftmost, and followed by the versions corrupted by impulse signals generated using spectral impulse noise model. The probability threshold are $T = 0.05, 0.15$.

3.3 More Examples

The use of the obtained dataset of spectral impulse noise is not limited to images containing uniform regions. In Fig. 7 we show several cutouts taken from hyperspectral images of different paintings. In the case of such images, a pixel that is corrupted by spectral impulse noise will be corrupted by an impulse signal that is taken from the dataset and has the most similarity to the original signal. However, as the number of colors are reduced to patches that are available in our database, a weak density is obtained in spectral space and consequently some color noise are not processed at a sufficient realistic level. Such case is illustrated in the green images shown in Fig. 7.

4 Application for Filtering Assessment

The main objective of this work on spectral noise model construction is to compare the performance of spectral image processing tools under controlled set-

Table 3. Distortion measure of several images before and after filtering process using Vector Median Filter embedding ECS distance. The corrupting impulse signals were generated with spectral impulse noise model and $T = 0.15$.

Pigment patch	Original		Salt & pepper		Spectral impulse	
	Before	After	Before	After	Before	After
Yellow, 21040	7.884	6.786	69.306	2.427	8.885	0.919
Orange, 21080	7.776	6.611	71.901	2.590	6.338	0.709
Red, 21110	7.875	7.028	72.849	1.524	6.877	0.509
Blue, 44450	10.868	7.835	58.291	2.582	10.871	0.522
Green, 44500	7.565	6.271	62.197	1.205	6.418	0.488
Purple, 45120	8.789	6.657	62.428	2.251	7.645	0.621

tings. Therefore in this section, we provide an application of the noise model construction on the assessment of spectral filtering performance. Vector Median Filter (VMF) by Astola et al. [3] is a median filtering algorithm suitable for multivariate data; its performance in the removal of impulse noise has been proven theoretically and numerically. We will use the artificial target images that have been constructed in Section 3.2 as filtering input; the ground truth is averaged image of the corresponding pigment patch.

In Table 3 distortion measures of several images before and after VMF are provided. For the original spectral images, VMF does not result in large modifications. VMF is effective for removing uniformly distributed impulse signals, while the distribution of variations in these images is certainly not uniform, for example see Fig. 3. Thus, VMF is not able to modify further the initial content of the images. When target images are corrupted with salt-and-pepper noise ($T = 0.15$), the initial distortion values are increased with ratio of ≈ 10. Nevertheless, the filtering impact allows to obtain images with reduced distortions compared to their corresponding original images, i.e. ratio of ≈ 20. In the case of the proposed spectral impulse noise model, the initial distortion measure is similar from the original real spectral images and the filtering process is able to reduce it with ratio of ≈ 9. Finally, the proposed spectral impulse noise model modifies the initial local statistics of the images, i.e. 30% of pixels in a local neighborhood are corrupted when $T = 0.15$, and thus simplifies the filtering process of the images as shown by the corresponding distortion measures for the original/ corrupted and filtered images.

5 Conclusion

Having a realistic model of spectral noise is crucial in order to assess the performance of spectral image processing tools. We have shown that theoretical models without inter-channel correlations are not suitable to model spectral noise, as theoretical models provide us with unrealistic aspect and behavior of spectral data. In this work we proposed a suitable spectral noise model using spectral database of uniform color/ pigment patches, which answers the challenge of identifying spectral noise model. This noise construction allows to produce realistic

model that is suitable for the assessment of spectral filtering algorithms performances. The limitation of this model is due to the reduced number of uniform color patches that are available in our database. However, by adding more color patches into the database such limit can be overcome and will eventually enable us to produce more complex spectral noise.

Acknowledgments. Authors would like to thank Norsk Elektro Optikk AS (NEO) for providing the hyperspectral scanner HySpex and the hyperspectral images of uniform pigment patches.

References

1. Norsk Elektro Optikk AS: HySpex. http://www.neo.no/hyspex/
2. Alajlan, N., Jernigan, E.: An effective detail preserving filter for impulse noise removal. In: Campilho, A.C., Kamel, M.S. (eds.) ICIAR 2004. LNCS, vol. 3211, pp. 139–146. Springer, Heidelberg (2004)
3. Astola, J., Haavisto, P., Neuvo, Y.: Vector median filters. Proceedings of the IEEE **78**(4), 678–689 (1990)
4. Bar, L., Brook, A., Sochen, N., Kiryati, N.: Color image deblurring with impulsive noise. In: Paragios, N., Faugeras, O., Chan, T., Schnörr, C. (eds.) VLSM 2005. LNCS, vol. 3752, pp. 49–60. Springer, Heidelberg (2005)
5. Celebi, M.E., Kingravi, H.A., Aslandogan, Y.A.: Nonlinear vector filtering for impulsive noise removal from color images. Journal of Electronic Imaging **16**(3), 033008-1–033008-21 (2007)
6. Chan, R., Ho, C.W., Nikolova, M.: Salt-and-pepper noise removal by median-type noise detectors and detail-preserving regularization. IEEE Transactions on Image Processing **14**(10), 1479–1485 (2005)
7. Justusson, B.J.: Median filtering: Statistical properties. Two Dimensional Digital Signal Processing **2**, 161–196 (1981)
8. Kober, V., Mozerov, M., Álvarez-Borrego, J.: Automatic removal of impulse noise from highly corrupted images. In: Sanfeliu, A., Cortés, M.L. (eds.) CIARP 2005. LNCS, vol. 3773, pp. 34–41. Springer, Heidelberg (2005)
9. Nair, M.S., Revathy, K., Tatavarti, R.: Removal of salt-and pepper noise in images: a new decision-based algorithm. In: Proceedings of the International MultiConference of Engineers and Computer Scientists (IMECS) I, pp. 19–21 (2008)
10. Nowicki, K.J., Edwards, C.S., Christensen, P.R.: Removal of salt-and-pepper noise in THEMIS infrared radiance and emissivity spectral data of the martian surface. IEEE-Whispers Transactions (2013, in press)